±30° from the oxygen rows. Thus, as atoms at the interfaces of semiconductor nanocrystals are expected to preferentially replace atoms in the cation sites of the matrix, our observations are in accord with simple atomistic models.

These results have important implications for epitaxial semiconductor films grown on the surface of alumina and spinel substrates. Early investigations of silicon-on-sapphire (SOS) films grown on α-Al_2O_3(0001) surfaces reported inconsistent results and no explanation has emerged[14]. To resolve these discrepancies, we note that the reported orientations for silicon films grown on basal-plane sapphire or spinel substrates generally correspond either to the α-type or to the γ-type alignment observed for our embedded precipitates. On the basis of these observations and symmetry considerations, we postulate that the origin of the inconsistencies in previous SOS reports lies in the substrate surface preparation and reconstruction. Surface-damaged sapphire substrates are known to present a spinel-like growth surface[15] and hence may generate γ-oriented epitaxial films, whereas sapphire-terminated surfaces should yield α-oriented epitaxial films. Our results suggest that, as has been accomplished by other approaches[16], it will be possible to pattern different film orientations on a single sapphire substrate.

Compound semiconductor nanocrystals offer an even broader range of possible structural modifications than single-component semiconductors. In addition to the size and orientation effects illustrated above for diamond-cubic, elemental semiconductors, we have found that it is possible to control the lattice structure for compound semiconductor nanocrystals. These results are of importance because many compound semiconductors, such as CdSe and CdS, possess direct or continuously tunable energy gaps with superior electro-optic properties[3,17,18]. Structurally, bulk CdSe and CdS can be stabilized at room temperature and pressure in either the hexagonal wurtzite (W) structure or the cubic zincblende structure (ZB). The structural relation between W and ZB can be represented as ABABAB … stacking versus ABCABC … stacking and hence is analogous to the α–γ relation of the oxygen planes in alumina. Previous studies have reported the synthesis of W as well as ZB CdSe nanocrystals[19]. However, after a detailed, quantitative analysis, Bawendi *et al.*[18] concluded that nanocrystals previously identified as ZB structure through visual inspection of powder diffraction patterns are actually better fitted by a random stacking sequence of the close-packed planes. In light of this result, there seems to be no previous (unambiguous) identification of CdSe nanocrystals with the ZB structure. Here, we have the experimental advantage of oriented nanocrystals; therefore, we can scan a particular direction in reciprocal space, rather than rely on a powder average.

Figure 3 shows X-ray scans from CdSe nanocrystals in alumina taken along a direction in reciprocal space specifically chosen to probe the stacking sequence. In terms of W coordinates, these scans are along the [0001] direction through the $(10\bar{1}l)$ reciprocal lattice positions. Indexed in this way, peaks at integral positions indicate the W structure whereas peaks at 1/3 integral positions indicate the ZB structure. The sample in Fig. 3a was implanted at 600 °C and contains CdSe nanocrystals with the W structure, whereas the substrate in Fig. 3b was held at room temperature and contains nanocrystals with the ZB structure. Thus, W nanocrystals are formed in the hexagonal α-alumina host, and ZB nanocrystals are formed in the cubic γ-alumina substrate. We conclude that the nanocrystal lattice structure directly mimics the symmetry of the matrix in which it is formed.

The ability to control the microstructure of semiconductor nanocrystals using ion beams provides opportunities for creating novel devices, and can be generalized to other substrates or other synthesis techniques. Many technologically important materials (ZrO_2, SiO_2, NiAl, YBaCuO, $MoSi_2$ and so on) have metastable phases and represent prime candidates for consideration as substrates[20]. Furthermore, we expect that similar effects will prove useful for other types of precipitates, including magnetic materials and ferroelectrics where anisotropy effects can be exploited using orientational control. Future studies will emphasize techniques for creating nanocrystals with better size uniformity. As self-ordered void arrays are known to form in irradiated sapphire[21], it is likely that ion implantation techniques can be developed to produce self-organized nanocrystals with uniform sizes. □

Received 8 May; accepted 30 September 1997.

1. Service, R. F. Small clusters hit the big time. *Science* **271,** 920–922 (1996).
2. Siegal, R. W. Creating nanophase materials. *Sci. Am.* **275,** 74–79 (1996).
3. Brus, L. Quantum crystallites and nonlinear optics. *Appl. Phys.* **A53,** 465–474 (1991).
4. Nirmal, M. *et al.* Fluorescence intermittency in single cadmium selenide nanocrystals. *Nature* **383,** 802–804 (1996).
5. Shimizu-Iwayama, T. *et al.* Visible photoluminescence related to Si precipitates in Si^+-implanted SiO_2. *J. Phys.: Condens. Matter* **5,** L375–L380 (1993).
6. White, C. W. *et al.* Encapsulated nanocrystals and quantum dots formed by ion beam synthesis. *Nucl. Instr. Meth.* **B127/128,** 545–552 (1997).
7. Min, K. S. *et al.* The role of quantum-confined excitons vs defects in the visible luminescence of SiO_2 films containing Ge nanocrystals. *Appl. Phys. Lett.* **68,** 2511–2513 (1996).
8. Reed-Hill, R. E. *Physical Metallurgy Principles* (Van Nostrand, New York, 1973).
9. White, C. W. *et al.* Ion implantation and annealing of crystalline oxides. *Mater. Sci. Rep.* **4,** 41–146 (1989).
10. Yu, N., McIntyre, P. C., Nastasi, M. & Sickafus, K. High-quality epitaxial growth of γ-alumina sapphire induced by ion-beam bombardment. *Phys. Rev.* **B52,** 17518–17522 (1995).
11. Pope, S. G. & Cochran, J. K. Mechanical properties of silicon ion implanted and annealed sapphire and polycrystalline alumina. *J. Mater. Eng.* **11,** 133–139 (1989).
12. Shimizu-Iwayama, T., Niimi, T., Nakao, S. & Saitoh, K. Investigations on the formation of SiO_2 in Si^+-implanted Al_2O_3. *Jpn. J. Appl. Phys.* **32,** L1451–L1453 (1993).
13. Voorhees, P. W. Ostwald ripening of two-phase mixtures. *Annu. Rev. Mater. Sci.* **22,** 197–215 (1992).
14. Filby, J. D. & Nielsen, S. Single-crystal films of silicon on insulators. *Brit. J. Appl. Phys.* **18,** 1357–1382 (1967).
15. Bursill, L. A. & Lin, P. J. Monolayer reconstruction on polar surfaces of ruby. *Phil. Mag.* **A60,** 307–320 (1989).
16. Angell, M. J. *et al.* Growth of alternating ⟨100⟩/⟨111⟩-oriented II–VI regions for quasi-phase-matched nonlinear optical devices on GaAs substrates. *Appl. Phys. Lett.* **64,** 3107–3109 (1994).
17. Colvin, V. L., Schlamp, M. C. & Alivisatos, A. P. Light-emitting diodes made from cadmium selenide nanocrystals and a semiconducting polymer. *Nature* **370,** 354–356 (1994).
18. Bawendi, M. G., Kortan, A. R., Steigerwald, M. L. & Brus, L. X-ray structural characterization of larger CdSe semiconductor clusters. *J. Chem. Phys.* **91,** 7282–7290 (1989).
19. Bandaranayake, R. J. *et al.* Structural phase behavior in II–VI semiconductor nanoparticles. *Appl. Phys. Lett.* **67,** 831–833 (1995).
20. Chou, T. C. & Nieh, T. G. Microstructural characteristics of layered metastable phases. *Scripta Met. Mater.* **26,** 1895–1900 (1992).
21. Lee, W. E., Jenkins, M. L. & Pells, G. P. The influence of helium doping on the damage microstructure of heavy-ion irradiated α-Al_2O_3. *Phil. Mag.* **A51,** 639–659 (1985).

Acknowledgements. This research was sponsored by Division of Materials Sciences, US Department of Energy, with Lockheed Martin Energy Research Corporation.

Correspondence should be addressed to J.D.B. (e-mail: xry@ornl.gov).

Facile synthesis of block copolypeptides of defined architecture

Timothy J. Deming

Departments of Materials and Chemistry, University of California, Santa Barbara, Santa Barbara, California 93106, USA

Many natural polymeric materials (particularly structural proteins) display a hierarchy of structure over several length scales. Block copolymers are able to self-assemble into ordered nanostructures[1,2], but the random-coiled nature of their polymer chains usually suppresses any further levels of organization. The use of components with regular structures, such as rigid-rod polymers, can increase the extent of spatial organization in self-assembling materials[3]. But the synthesis of such polymeric components typically involves complicated reaction steps that are not suitable for large-scale production. Proteins form hierarchically organized structures in which the fundamental motifs are generally α-helical coils and β-sheets[4]. Attempts to synthesize polypeptides with well-defined amino-acid sequences, which might adopt similar organized structures, have been plagued by unwanted side reactions[5] that give rise to products with a wide range of molecular weights[6–10], hampering the formation of well-defined peptide block copolymers[11–17]. Here I describe a polymer-

ization strategy that overcomes these difficulties by using organonickel initiators which suppress chain-transfer and termination side reactions. This approach allows the facile synthesis of block copolypeptides with well-defined sequences, which might provide new peptide-based biomaterials with potential applications in tissue engineering, drug delivery and biomimetic composite formation.

Small peptide sequences, typically less than 100 residues in length, are most conveniently prepared using stepwise solid-phase synthesis. However, the chemical synthesis of high-molecular-weight polypeptides is most directly accomplished by the ring-opening polymerization of α-aminoacid-*N*-carboxyanhydride (NCA) monomers (equation (1))[5,11,12].

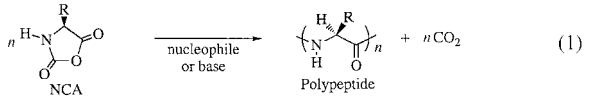

(1)

NCAs are readily prepared, typically in a single step from commercially available amino acids, and polymerize in the presence of nucleophiles or bases to give polypeptides in good yield without racemization of chiral centres. The main limitation of NCA polymerizations using conventional initiators (such as hexylamine or sodium methoxide) is that they are plagued by chain-breaking transfer and termination reactions which prevent formation of block copolymers[11–15]. For more than 40 years, the mechanisms of NCA polymerization have been under intensive study so that problematic side reactions could be eliminated[5,11,12]. These investigations have been severely hindered by the complexity of the polymerizations, which can proceed through multiple pathways[11,12].

Because there is some chain-length control at low ratios of monomer to initiator, there have been claims that amine-initiated polymerizations can be used to prepare block copolypeptides[6–10]. These copolymers were often only subjected to limited characterization (for example, amino acid compositional analysis) and, as such, their structures, and the presence of homopolymer contaminants, were not conclusively determined. Copolymers that had been subjected to chromatography showed polymodal molecular-weight distributions containing substantial high- and low-molecular-weight fractions[6]. The compositions of these copolymers were found to be very different from the initial monomer feed compositions and varied widely for different molecular-weight fractions. It appears that most, if not all, block copolypeptides prepared using amine initiators have structures different from those predicted from the monomer feed compositions and probably have considerable homopolymer contamination due to chain-breaking reactions.

Successful synthesis of block copolypeptides requires the elimination of side reactions in favour of the chain-growth process (living polymerization), thus allowing multiple monomer additions to each chain[18,19]. I have approached this problem by using the versatile chemistry of transition metals to mediate the addition of monomers to the active polymer chain-ends[16]. The wide range of selective chemical transformations and polymerizations that are catalysed by transition-metal complexes attests to the potential of this approach[20]. I initially attempted to use metal coordination complexes of conventional amine initiators to control the polymerizations[17]. Use of metal–amine complexes for polymerization of γ-benzyl-L-glutamate *N*-carboxyanhydride, Glu-NCA, allowed the preparation of poly(γ-benzyl-L-glutamate), PBLG, with narrow molecular weight distribution (M_w/M_n = 1.05–1.10) and some control over molecular weight. However, typical problems inherent in polymerizations initiated by primary amines (slow propagation and chain-transfer reactions) prevented use of these initiators for preparation of block copolypeptides.

I now report the discovery of a new class of initiators based on organonickel compounds which are able to eliminate significant competing termination and transfer steps from NCA polymerizations, and allow preparation of well-defined block copolypeptides. Formation of the initiator results from the reaction of an NCA monomer with the zero-valent nickel complex bipyNi(COD); bipy = 2,2′-bipyridyl, COD = 1,5-cyclooctadiene. This reaction is similar to the oxidative addition of cyclic anhydrides to zero-valent nickel which yields divalent nickel metallacycles (equation (2))[21–23].

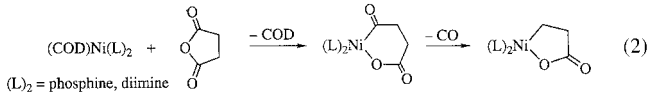

(2)

Activation and polymerization of NCAs through oxidative ring opening of the anhydride, however, is without precedent. Successful polymerization of L-proline NCA, which lacks a proton bound to

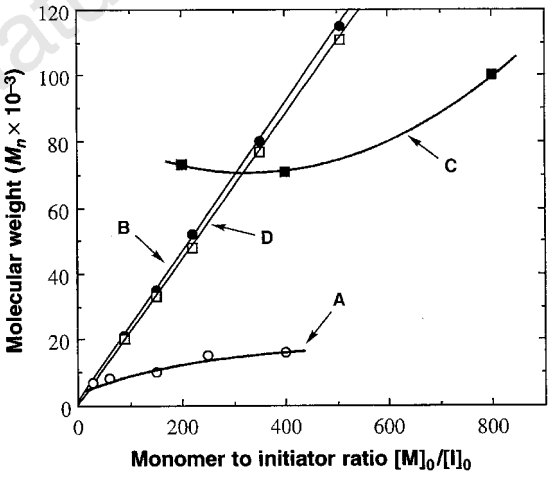

Figure 1 Comparison of the abilities of different initiators to control molecular weight of PBLG as a function of initiator concentration in polymerizations of Glu-NCA: **A**, phenethylamine initiator; **B**, bipyNi(COD) initiator; **C**, sodium *tert*-butoxide initiator; **D**, theoretical molecular weight calculated from $[M]_0/[I]_0$. All polymerizations were run in anhydrous DMF at 25 °C for 1 day in sealed tubes. Molecular weight (M_n) was determined by tandem GPC/light scattering in 0.1M LiBr in DMF at 60 °C.

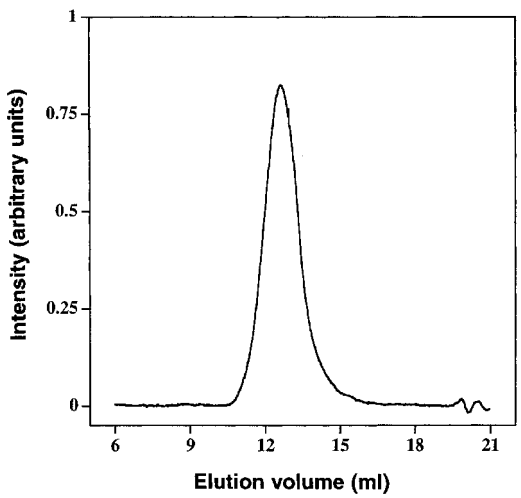

Figure 2 Chromatogram of a $PBLG_{0.78}$-*b*-$PZLL_{0.22}$ diblock copolymer prepared by sequential addition of Lys-NCA and Glu-NCA to bipyNi(COD) initiator in DMF. The polymerization mixture was injected directly into the GPC, eluted using 0.1 M LiBr in DMF at 60 °C through 10^5 Å and 10^3 Å Phenomenex 5 μm columns, and detected with a Wyatt DAWN DSP light-scattering detector and Wyatt Optilab DSP.

Table 1 Preparation and analysis of block copolypeptides

		First segment†		Diblock copolymer‡		
First monomer*	Second monomer*	M_n	M_w/M_n	M_n	M_w/M_n	Yield (%)§
52 Lys-NCA	181 Glu-NCA	15,000‖	1.12	66,000¶	1.21	95
90 Glu-NCA	78 Lys-NCA	28,500#	1.12	52,700**	1.13	93
104 Lys-NCA	40 Leu-NCA	29,500‖	1.13	34,000‖	1.20	93
182 Glu-NCA	90 Pro-NCA	57,600#	1.07	86,000#	1.14	92
120 Glu-NCA	40 Leu-NCA	38,000#	1.08	79,000#	1.13	96

Polymerization initiator was bipyNi(COD) in DMF in all cases. Molecular weight (M_n) and polydispersity (M_w/M_n) were determined by tandem GPC/light scattering in 0.1M LiBr in DMF at 60 °C using dn/dc values (c = concentration) measured in this solvent at $\lambda_0 = 633$ nm.
* First and second monomers added stepwise to the initiator; number indicates equivalents of monomer per bipyNi(COD). Leu-NCA = L-leucine-*N*-carboxyanhydride. Pro-NCA = L-proline-*N*-carboxyanhydride.
† Molecular weight and polydispersity after polymerization of the first monomer.
‡ Molecular weight and polydispersity of the complete block copolymer.
§ Total isolated yield of block copolymer.
‖ $dn/dc = 0.123\ \mathrm{mL\,g^{-1}}$.
¶ $dn/dc = 0.108\ \mathrm{mL\,g^{-1}}$.
# $dn/dc = 0.104\ \mathrm{mL\,g^{-1}}$.
** $dn/dc = 0.115\ \mathrm{mL\,g^{-1}}$.

nitrogen, using bipyNi(COD) supports the hypothesis of oxidative addition across the anhydride bond, rather than reaction at the N–H bond.

As NCAs are unsymmetrical anhydrides, the oxidative addition of NCAs can yield two distinct isomeric products (equation (3)).

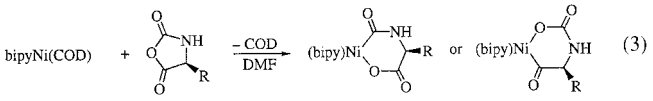

(3)

I found that the addition of NCAs to nickel was completely regioselective for ring opening across the O–C_5 bond. Reaction of bipyNi(COD) with $^{13}C_2$-L-leucine NCA and $^{13}C_5$-L-leucine NCA yielded oxidative addition products and bipyNi$(CO)_2$ which were examined by ^{13}C NMR and Fourier-transform infrared (FTIR) spectroscopy. Detection of bipyNi($^{12}CO_2$) (FTIR (tetrahydrofuran): CO stretch = 1,978, 1,904 $\mathrm{cm^{-1}}$) from the reaction of $^{13}C_2$-L-leucine NCA, and bipyNi($^{13}CO)_2$ (FTIR(THF): CO stretch = 1,934, 1,862 $\mathrm{cm^{-1}}$; ^{13}C NMR(DMF-d_7): 198 p.p.m. (Ni-CO)) from the reaction of $^{13}C_5$-L-leucine NCA identified the regiochemistry of the product (equation (4)).

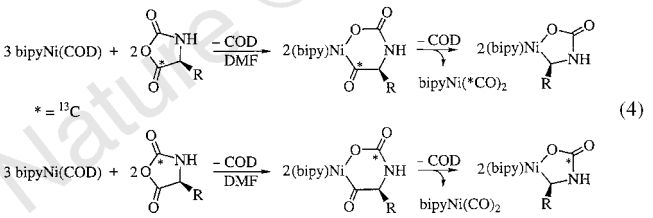

(4)

In dimethylformamide (DMF), a good solvent for polypeptides, this addition product was found to be completely active for polymerization of additional NCA monomers.

I analysed the efficiency of the initiator through polymerization experiments with Glu-NCA. The resulting polymer, PBLG, is a α-helical in many solvents, has been extensively studied and is readily characterized[24]. The number-average molecular weight of PBLG samples formed using bipyNi(COD) in DMF was found to increase linearly as function of the intial monomer-to-initiator ratios, indicating the absence of chain-breaking reactions[18,19]. Such control over polypeptide molecular weight is a substantial improvement over conventional NCA polymerization systems (Fig. 1). The polymers possessed narrow molecular-weight distributions (M_w/M_n = 1.05–1.15) and were obtained in excellent yields (95–99% isolated). Kinetic analysis also showed that the polymerizations were well behaved. The polymerizations were first order in monomer concentration over four half-lives in DMF (observed rate constant = $2.7(1) \times 10^{-4}\ \mathrm{s^{-1}}$ at 298 K; [bipyNi(COD)] = 0.67 mM) showing none of the complexities of traditional NCA polymerizations. The initiating system displays all of the characteristics of a living chain-growth process for Glu-NCA. Analysis of other NCA monomers (such as ε-carbobenzyloxy-L-lysine *N*-carboxyanhydride, Lys-NCA) also yielded controlled polymerizations, illustrating the general utility of the initiating system for preparation of well-defined block copolypeptides with a variety of architectures.

I synthesized diblock copolymers composed of amino-acid components γ-benzyl-L-glutamate and ε-carbobenzyloxy-L-lysine. The polymers were prepared by addition of Lys-NCA to bipyNi(COD) in DMF to afford living poly(ε-carbobenzyloxy-L-lysine), PZLL, chains with organometallic end-groups capable of further chain growth. Glu-NCA was added to these polymers to yield the PBLG–PZLL block copolypeptides. The evolution of molecular weight through each stage of monomer addition was analysed using gel permeation chromatography (GPC), and data are given in Table 1. Molecular weight was found to increase as expected on growth of each block of copolymer while polydispersity remained low, indicative of successful copolymer formation[25]. The chromatograms of the block copolypeptides showed single sharp peaks illustrating the narrow distribution of chain lengths (Fig. 2). Copolypeptide compositions were easily adjusted by variation of monomer feed compositions, both being equivalent. Successful preparation of copolypeptides of reverse sequence (PZLL–PBLG) and of triblock structure (such as $PBLG_{0.39}$–*b*-$PZLL_{0.22}$–*b*-$PBLG_{0.39}$; M_n = 256,000, M_w/M_n = 1.15) illustrate the potential for sequence control using the nickel initiator.

Block copolymerizations were not restricted to the highly soluble polypeptides PBLG and PZLL. I have also prepared copolypeptides containing L-leucine and L-proline, both of which form homopolymers which are insoluble in most organic solvents (such as DMF). Data for these copolymerizations are given in Table 1. Because of the solubilizing effect of the PBLG and PZLL blocks, all of the products were soluble in reaction media, indicating the absence of any homopolymer contaminants. The block copolymers containing L-leucine were found to be strongly associating in 0.1M LiBr in DMF, a good solvent for PBLG and PZLL. Once side-chain protecting groups are removed, the assembly properties of these materials are expected to make them useful as tissue engineering scaffolds, drug carriers and morphology-directing components in biomimetic composite formation. □

Received 27 June; accepted 7 October 1997.

1. Hillmyer, M. A. *et al.* Complex phase behavior in solvent-free nonionic surfactants. *Science* **271,** 976–978 (1996).
2. Matsen, M. W. & Bates, F. S. Origins of complex self-assembly in block copolymers. *Macromolecules* **29,** 7641–7644 (1996).
3. Stupp, S. I. *et al.* Supramolecular materials: self-organized nanostructurs. *Science* **276,** 384–389 (1997).
4. Fasman, G. D. *Prediction of Protein Structure and the Principles of Protein Conformation* (Plenum, New York, 1989).
5. Bamford, C. H., Elliot, A. & Hanby, W. E. *Synthetic Polypeptides* (Academic, New York, 1956).
6. Cardinaux, F., Howard, J. C., Taylor, G. T. & Scheraga, H. A. Block copolymers of amino acids. I. Synthesis and structure of copolymers of L-alanine or L-phenylalanine with D,L-lysine-d_7 or D,L-lysine. *Biopolymers* **16,** 2005–2028 (1977).

7. Howard, J. C., Cardinaux, F. & Scheraga, H. A. Block copolymers of amino acids. II. Physicochemical data on copolymers containing L-alanine or L-phenylalanine. *Biopolymers* **16,** 2029–2051 (1977).
8. Gratzer, W. B. & Doty, P. A conformational examination of poly-L-alanine and poly-D,L-alanine in aqueous solution. *J. Am. Chem. Soc.* **85,** 1193–1197 (1963).
9. Inoue, K. *et al*. Preparation and conformation of hexaarmed star poly(β-benzyl-L-aspartates) utilizing hexakis(4-aminophenoxy) cyclotriphosphazene. *J. Am. Chem. Soc.* **116,** 10783–10784 (1994).
10. Kubota, S. & Fasman, G. D. The β conformation of polypeptides of valine, isoleucine, and threonine in solution and solid-state: optical and infrared studies. *Biopolymers* **14,** 605–631 (1975).
11. Kricheldorf, H. R. *α-Aminoacid-N-Carboxyanhydrides and Related Materials* (Springer, New York, 1987).
12. Kricheldorf, H. R. in *Models of Biopolymers by Ring-Opening Polymerization* (ed. Penczek, S.) (CRC, Boca Raton, 1990).
13. Idelson, M. & Blout, E. R. Polypeptides XV. Infrared spectroscopy and the kinetics of the synthesis of polypeptides: primary amine initiated reactions. *J. Am. Chem. Soc.* **79,** 3948–3957 (1957).
14. Idelson, M. & Blout, E. R. Polypeptides XVIII. A kinetic study of the polymerization of amino acid *N*-carboxyanhydrides initiated by strong bases. *J. Am. Chem. Soc.* **80,** 2387–2393 (1958).
15. Lundberg, R. D. & Doty, P. Polypeptides XVII. A study of the kinetics of the primary amine-initiated polymerization of *N*-carboxyanydrides with special reference to configurational and stereochemical effects. *J. Am. Chem. Soc.* **79,** 3961–3972 (1957).
16. Deming, T. J. Polypeptide materials: new synthetic methods and applications. *Adv. Mater.* **9,** 299–311 (1997).
17. Deming, T. J. Transition metal–amine initators for preparation of well-defined poly(γ-benzyl-L-glutamate). *J. Am. Chem. Soc.* **119,** 2759–2760 (1997).
18. Fetters, L. J. in *Encyclopedia of Polymer Science and Engineering* 2nd edn 19–25 (Wiley-Interscience, New York, 1987).
19. Webster, O. Living polymerization methods. *Science* **251,** 887–893 (1991).
20. Collman, J. P., Hegedus, L. S., Norton, J. R. & Finke, R. G. *Principles and Applications of Organotransition Metal Chemistry* 2nd edn (University Science, Mill Valley, 1987).
21. Uhlig, E., Fehske, G. & Nestler, B. Z. Reaktionen cyclischer Carbonsaueureanhydride mit (α,α′-Dipyridyl)-(cyclooctadien-1,5)-nickel. *Anorg. Allg. Chem.* **465,** 141–146 (1980).
22. Sano, K., Yamamoto, T. & Yamamoto, A. Preparation of Ni- or Pt-containing cyclic esters by oxidative addition of cyclic carboxylic anhydrides and their properties. *Bull. Chem. Soc. Jpn* **57,** 2741–2747 (1984).
23. Castaño, A. M. & Echavarren, A. M. Reactivity of a nickelacycle derived from aspartic acid: alkylations, insertions, and oxidations. *Organometalics* **13,** 2262–2268 (1994).
24. Block, H. *Poly(γ-benzyl-L-glutamate) and Other Glutamic Acid Containing Polymers* (Gordon and Breach, New York, 1983).
25. Noshay, A. & McGrath, J. E. *Block Copolymers* (Academic, New York, 1977).

Correspondence and requests for materials should be addressed to T.J.D. (e-mail: tdeming@engineering.ucsb.edu).

Interrelated influence of iron, light and cell size on marine phytoplankton growth

William G. Sunda & Susan A. Huntsman

National Marine Fisheries Service, 101 Pivers Island Road, Beaufort, North Carolina 28516, USA

The sub-optimal growth of phytoplankton and the resulting persistence of unutilized plant nutrients (nitrate and phosphate) in the surface waters of certain ocean regions has been a long-standing puzzle[1,2]. Of these regions, the Southern Ocean seems to play the greatest role in the global carbon cycle[3,4], but controversy exists as to the dominant controls on net algal production. Limitation by iron deficiency[4,5], light availability[1,6,7] and grazing by zooplankton[2] have been proposed. Here we present the results from culture experiments showing that the amount of cellular iron needed to support growth is higher under lower light intensities, owing to a greater requirement for photosynthetic iron-based redox proteins by low-light acclimatized algae. Moreover, algal iron uptake varies with cell surface area, such that the growth of small cells is favoured under iron limitation, as predicted theoretically[8]. Phytoplankton growth can therefore be simultaneously limited by the availability of both iron and light. Such a co-limitation may be experienced by phytoplankton in iron-poor regions in which the surface mixed layer extends below the euphotic zone—as often occurs in the Southern Ocean[6,7]—or near the bottom of the euphotic zone in more stratified waters. By favouring the growth of smaller cells, iron/light co-limitation should increase grazing by microzooplankton, and thus minimize the loss of fixed carbon and nitrogen from surface waters in settling particles[9,10].

We examined the iron uptake and growth dynamics of coastal diatoms (*Thalassiosira pseudonana* and *T. weissflogii*) and dinoflagellates (*Prorocentrum minimum* and *P. micans*) representing a range of cell diameters (3.5 to 30–32 μm) (Fig. 1). Experiments were run at light intensities of 500 and 50 μeinstein m^{-2} s^{-1} for *T. pseudonana* and *P. minimum* and at the higher intensity only for the other two species. The cells were grown at 20 °C on a 14 : 10 h light : dark cycle in EDTA-metal ion buffered media[11]. We measured the steady-state cellular Fe, Fe uptake rates, chlorophyll *a*, cell size

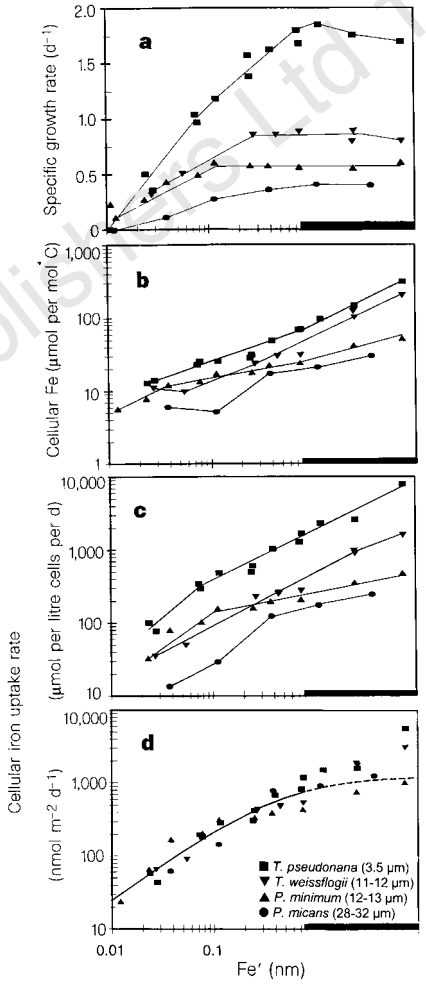

Figure 1 Relationships among specific growth rate, intracellular Fe : C (measured with radiotracers), Fe uptake rate (normalized to cell volume and equivalent spherical surface area), and [Fe′] for coastal eukaryotes of varying mean diameters grown at 500 μE m^{-2} s^{-1} (here μE indicates microeinstein). The 36‰ salinity media was enriched with EDTA/trace metal ion buffers and 32 μM $NaNO_3$, 2 μM Na_2HPO_4, 40 μM Na_2SiO_3, 10 nM Na_2SeO_3, 0.074 nM vitamin B_{12}, 0.4 nM biotin and 60 nM thiamin. Solid bar on the *x*-axis represents the region where Fe hydroxides are observed to precipitate[11]. Horizontal dimensions in all cases are proportional to total Fe. [Fe′] is the mean value over a 14 : 10 light : dark cycle and equals total dissolved Fe times 0.0025, 0.00166 and 0.00132 at light intensities of 500, 160 and 50 μE m^{-2} s^{-1}. The solid curve in **d** gives the modelled saturation curve as fitted to equation (1) by nonlinear regression ($R^2 = 0.90$) using data for [Fe′] ≤ 0.75 nM. Results presented here are mostly new, but also include some published[11] high-light data for *T. pseudonana*, *T. weissflogii* and *P. minimum*. The data include three separate experiments with *T. pseudonana*, and two each with *T. weissflogii* and *P. minimum*. A single *T. pseudonana* experiment with four Fe levels run in triplicate yielded mean standard deviations of ±3.2, 3.9, 8.5, 8.4 and 10% for specific growth rate, Fe : C, Fe per litre cell volume, and C- and volume-normalized uptake rates, respectively. Experimental procedures and analyses are as described previously[11].